Minutes-timescale 3D isotropic imaging of entire organs at subcellular resolution by content-aware compressed-sensing light-sheet microscopy

Chunyu Fang[1+], Tingting Chu[1+], Tingting Yu[2,3], Yujie Huang[4], Yusha Li[2], Peng Wan[2], Dan Wang[4], Xuechun Wang[1], Wei Mei[4*], Dan Zhu[2,3*] and Peng Fei[1*]

[1] *School of Optical and Electronic Information- Wuhan National Laboratory for Optoelectronics, Huazhong University of Science and Technology, Wuhan, 430074, China.*

[2] *Britton Chance center for Biomedical Photonics, Wuhan National Laboratory for Optoelectronics, Huazhong University of Science and Technology, Wuhan 430074, China.*

[3] *MoE Key Laboratory for Biomedical Photonics, Huazhong University of Science and Technology, Wuhan, 430074, China*

[4] *Department of Anesthesiology, Tongji Hospital, Tongji Medical College, Huazhong University of Science and Technology, Wuhan, 430030, China*

[+] *These authors contribute equally to this work*

[*] *Correspondence: wmei@hust.edu.cn; dawnzh@mail.hust.edu.cn; feipeng@hust.edu.cn*

Abstract

We here report on a compressed sensing-enabled Bessel light-sheet microscopy system able to achieve fast scalable mapping of entire organs at an isotropic subcellular resolution. A dual-side confocally-scanned Bessel light-sheet with a millimeter-to-centimeter tunable range was developed to illuminate regions-of-interest from a few cells to entire organs, providing uniform optical sectioning of deep tissues with 1-5 μm ultra-thin axial confinement. We also present a new computation pipeline termed content-aware compressed sensing (CACS), which can further improve the contrast and resolution of a 3D image based on a single input of its own, allowing satisfying spatial resolution with data acquisition shorten by two-orders of magnitude. Using this method, we can image any region-of-interest of a selected mouse brain at submicron isotropic resolution in seconds, after screening multiple whole brains in minutes, and then *in toto* reconstruct the digital whole brain (~400 mm^3) at a teravoxel scale with a short acquisition time of ~15 minutes. We also demonstrate subcellular-resolution minute-timescale dual-color imaging of neuromuscular junctions in thick mouse muscles. Various system-level cellular analyses, such as mapping cell populations at different brain sub-regions, tracing long-distance projection neurons over the entire brain, and calculating neuromuscular junction occupancy across whole tissue, were enabled by our high-throughput high-resolution imaging method.

Introduction

The comprehensive understanding of majority and singular cellular events, as well as their complex connections in whole organs and organisms, is one of the fundamental quests in biology. To extract the various cellular profiles of different physiological functions within specimens, three-dimensional (3D) high-resolution imaging is required throughout a mesoscale-sized volume. However, creating such a large-scale image dataset has posed significant challenges for current 3D light microscopy methods, which all show relatively small optical throughputs[1,2]. Furthermore, in thick mammalian organs, severe light scattering and attenuation greatly limit the complete extraction of signals from deep tissues. A common strategy for addressing these issues has been to use 3D tile stitching combined with tissue sectioning[2-5]. For example, both tiling confocal microscopy[6-9] and sequential two-photon tomography[10,11] (STPT) can three-dimensionally image mouse brain at subcellular resolution, but do so at the expense of a very long acquisition time due to the slow laser-point-scanning and mechanical slicing. Light-sheet microscopy[12-15] (LSM) in conjunction with advanced tissue clearing techniques[16-19] eliminates the need of mechanical slicing by instead applying a nondestructive light-sheet to selectively illuminate a thin plane of the sample. At the same time, the use of wide-field detection results in higher imaging throughput in comparison with the point-by-point scanning used in epifluorescence methods. Although light-sheet microscopy using a Gaussian-type hyperbolic light-sheet[2,13,20] has been successfully used for imaging large organ samples, a trade-off exists between the minimum thickness of the light-sheet and the confocal range over which it remains reasonably uniform. As a reference, when illuminating a range of 1 mm in length, an optimized Gaussian light-sheet diverges to a full-width at half-maximum (FWHM) thickness of 12.5 μm at either end, and is hence incapable of resolving fine neuronal fibers across a large volume of brain. Sweeping the light-sheet along the propagation direction can extend the confocal range, but the achieved axial resolution remains inadequate, and tissue scattering effects also limit its propagation range[21,22]. Bessel-type light-sheet microscopy[23-25] (LSM) can generate a thin and non-diverging light-sheet that can illuminate samples with a much larger field of view while maintaining high axial resolution. Considering the necessity of minimizing excitation from the side lobes of the Bessel beam[26,27], Bessel LSM

usually uses a high numerical-aperture (NA) detection objective with a small depth of focus to reduce the fluorescence excitation by the side lobes. Thus, it is mainly optimized for the imaging of a single or a few cells at deep subcellular resolution. However, as with epifluorescence methods that suffer from a trade-off between accuracy and scale, Gaussian and Bessel LSM systems still have limited optical throughput, which is far from adequate for obtaining high spatial resolution across a very large field of view (FOV)[28]. To image a whole mouse brain at single-cell resolution, a small step size and tile-stitching at high magnification are necessary to acquire trillions of sub-μm^3 voxels over a cm^3-sized volume[2,19]. Therefore, a long acquisition time of up to several days, as well as increased photobleaching to samples, still prevents more widespread applications of LSM to the high-resolution mapping of entire mammalian organs/organisms.

We here report on a large-FOV scanning Bessel light-sheet microscopy method combined with a post-computation procedure termed content-aware compressed sensing (CACS), to address the aforementioned challenges of limited resolution and throughput. This CACS-enabled Bessel light-sheet microscopy can overcome the limitations of anisotropic 3D resolution that hinder current whole-organ imaging techniques. Furthermore, our new microscopy technique computationally mitigates the trade-off between imaging speed and accuracy by achieving efficient super-resolution with a single measurement. We apply this method to high-throughput scalable anatomical imaging of whole mouse brain and thick mouse muscle to demonstrate its unique capabilities, such as the quick screening of multiple organs in real time, rapid interrogation of any region of interest within selected samples at isotropic subcellular resolution, and teravoxel high-resolution mapping of entire samples on a timescale of minutes. We also demonstrate system-level cellular profiling, such as cell population counting and tracing of neural projections.

Results

Zoomable, line-synchronized Bessel plane illumination microscopy

Our Bessel plane illumination microscope (**Supplementary Fig. 1**) sweeps a long circular Bessel beam in the *y* direction across the focal plane of the detection objective to create a large-

scale scanned light-sheet and yield an image at a single *z*-plane within the specimen. To suppress the laser attenuation/scattering from samples, we introduced two opposite plane illumination sources from dual sides of the brain. A macro-view microscope (Olympus MVX10) providing zoomable magnification from 1.26×/0.14 to 12.6×/0.5, together with a sCMOS camera (Hamamatsu ORCA-Flash4.0 V2) were used as the fluorescence detection unit, providing a tunable FOV from 1 to 10 mm and effective lateral resolution from ~1 μm to 10 μm for large specimens. To achieve isotropic resolution, we used a switchable excitation objective with an NA of 0.055–0.28 to form a tunable illuminating Bessel beam with axial extent and diffraction length matched with the varying lateral resolutions and FOV, respectively. Finally, to enable high-throughput volumetric imaging of specimen, a customized sample holder rapidly moved the sample across the light-sheet along the *z* direction, with plane images at different depths consecutively obtained. The holder can also flip the sample through 180° to allow imaging under two views, so that the acquired dual-view images can be fused to further suppress fluorescence depletion from deep tissue. Photographs of our self-built microscope are shown in **Supplementary Fig. 2**. The simple mode of operation involves sweeping the Bessel beam in the *y* direction to create a continuous sheet at each *z* plane. However, in this mode, the cross-sectional profile of the excitation sheet contains broad tails because of the combined influence of the side lobes[24] (**Supplementary Fig. 3**). Given the fact that the increase in depth-of-field is proportional to the square of the decrease in NA, the axial excitation from these side lobes is more likely to deteriorate the fluorescence detection in our low-to-middle magnification/NA setup (**Supplementary Figs. 4, 5**). A confocal slit was therefore formed by tightly synchronizing the sweeping Bessel beam with the rolling active pixel lines of the camera[29,30], to block the influence of residing fluorescence excited by the side lobes, and led to much less background (**Supplementary Figs. 3, 4, 6**). As a result, the microscopy system could produce sharp optical sectioning at a very large scale, for example, generating of a 1 × 1-mm illuminating light-sheet with a cross-sectional profile of ~1 μm in thickness, as compared with a ~10 μm Gaussian sheet covering the same FOV (**Supplementary Fig. 3**). When this wide and thin Bessel plane illumination combined with a matched FOV (12.6×) was applied to the imaging of cleared mouse brain tissue with green fluorescent protein (GFP)-labelled neurons (**Fig. 1c** and Methods), the maximum intensity projection in the *y*-*z* plane of the cortical area

showed axial resolution and contrast superior to those of wide-field and Gaussian plane illumination (**Fig. 1a, b**).

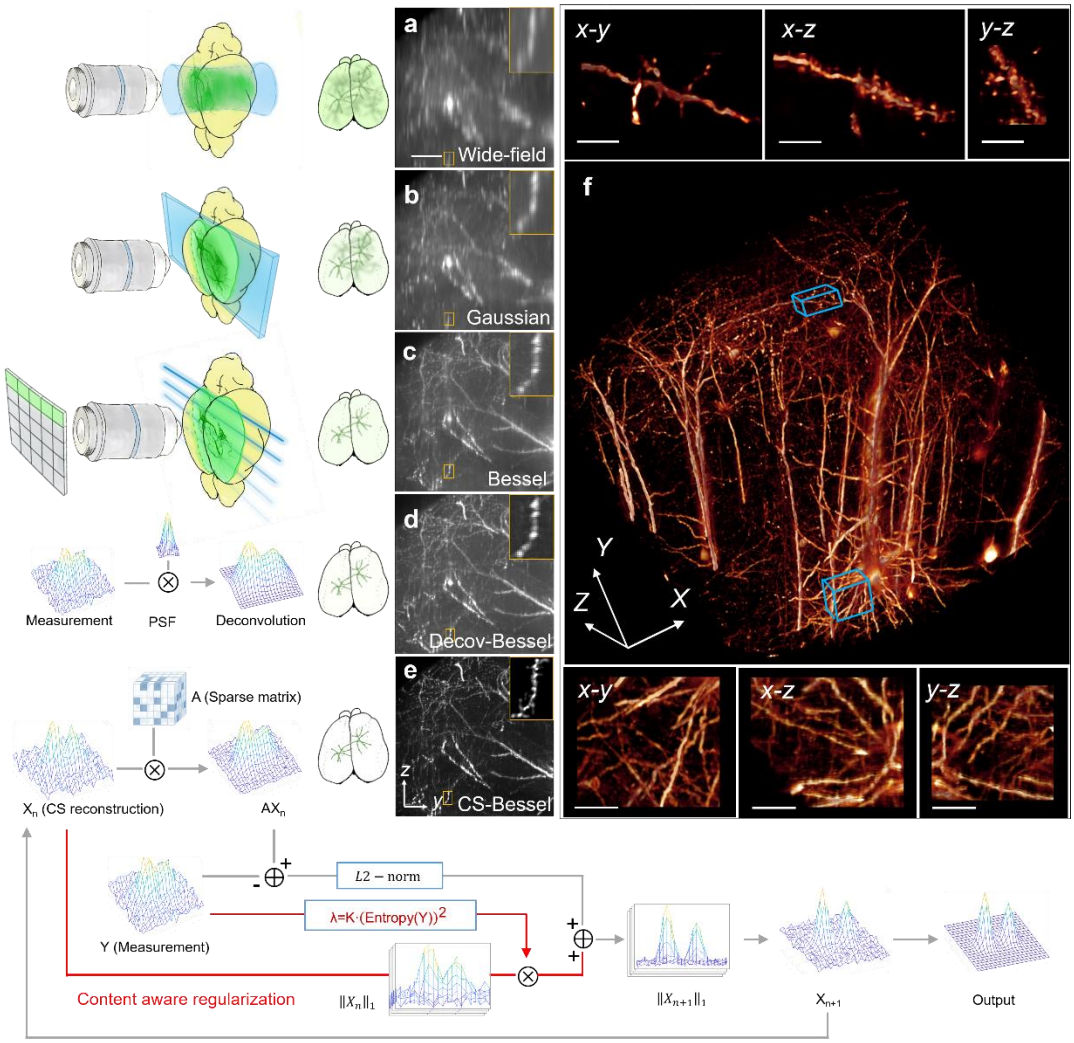

Fig. 1 | CACS Bessel plane illumination microscopy and other imaging modes. a, Epi-illumination mode (left) and maximum-intensity-projection (MIP) in the *y-z* plane (right) from a 3D image stack of a cleared transgenic mouse brain tissue with GFP labelled to the neurons (Thy1-GFP-M). **b**, Gaussian sheet mode (left), showing plane illumination at selective depth of brain, and *y-z* plane MIP (right) from the same sample shown in **a**. **c-e**, Raw-, deconvolution- and CACS- modes under synchronized Bessel illumination geometry, showing sharper optical sectioning (**c**, left) with regular deconvolution (**d**, left) and CACS computation (**e**, left) further applied. The *y-z* plane MIPs by each mode are accordingly shown in right columns. Scale bar, 20 µm. **f**, Volume rendering of GFP-labelled neurons in a cleared mouse cortex tissue by CACS Bessel sheet mode. Insets: MIPs along orthogonal axes of the cubical volume of interest (blue boxes). Scale bar, 10 µm.

CACS Bessel plane illumination microscopy

The raw Bessel results may still show inadequate resolutions at relatively large FOVs, for

example, 1-4 μm for a 1-4 mm FOV under magnifications of 12.6× to 3.2×. Normally, the raw Bessel sheet data can be deconvolved with the appropriate point spread functions (PSFs), to slightly improve image quality (**Fig. 1d**). However, a more effective means to improve the contrast and resolution of a single measurement is compressed sensing (CS) computation, which is well-known for its ability to recover signals from incomplete measurements[31]. In its conventional light microscopy implementation, CS recovers degraded signals from camera pixilation (wide-field) or incomplete scanning (confocal), and reduced the acquisition time for each 2D frame[32,33]. It also used to improve signal quality for 2D speckle image in nonlinear structured illumination microscopy[34]. In Bessel light-sheet microscopy, the camera's under-sampling in the *x*-*y* plane and sparse *z*-excitation by thin plane illumination make it suitable for the application of compressed sensing (**Supplementary Fig. 5**). To adopt this approach to Bessel imaging, in which the signal sparsity and dynamic range may vary drastically within a large volume[35] (**Supplementary Figs. 7, 8**), for the first time we extended the CS computation to three dimensions and applied content-aware (CA) regularization that was highly adaptive to the signal characteristics (**Fig. 1e**). Using our CACS processing, we aimed to achieve a higher-quality image x from the raw large-scale Bessel image y, which shows inadequate resolution resulting from the voxelization and limited numerical aperture. The Bessel image y was first divided into multiple small volumes y_i to calculate the compressed sensing matrix A_i in sparse domain, and a parameter β based on the entropy representing the degree of signal disorder (**Supplementary Note 3**). A regularization factor λ_i is then determined from the calculated β, as well as a signal density index α, and these are applied to the regularization term $\sum_i x_i$. This content-aware regularization with appropriate λ_i balances the iterative signal reconstruction process between an overfitting result subject to excessive constraints from complicated signals and an under-fitting result with too spare signals accompanied by obvious artefacts that are difficult to further optimized by iteration (**Supplementary Fig. 9**). A higher-resolution image tile x_i can be recovered by finding the optimal solution of the following problem in the sparse Fourier domain:

$$\min(\|Ax - y\|^2 + \lambda \sum_i x_i) \tag{1}$$

Detailed descriptions of the CACS computation are shown in the Methods. The 3D CACS

computation made obvious improvements to the raw Bessel sheet data, with resolution and contrast superior to that achieved by traditional deconvolution (**Fig. 1e**). Finally, the multiple small CACS reconstruction y_i were stitched together to form the final high-resolution large-scale output (**Supplementary Fig. 10**). **Fig. 1f** shows a volume rendering of apical dendrites in a region of the cortex yielding sufficiently high isotropic 3D resolution and signal-to-noise ratio (SNR) to discern subcellular structures such as dendrite spines. Furthermore, although the demonstrated neurons were originally imaged at 12.6×, this strategy was verified as being applicable to lower magnifications, such as 3.2× and 1.6×, and to different types of signals such as fluorescent beads, showing similar improvements in comparison with the original images. Unlike multi-frame super-resolution imaging methods, which are powerful but suffer from the time expense of repeated measurements, the 3D CACS can provide an output with obvious improvement using only a single measurement as input. Therefore, it offers a good balance between the higher spatial resolution required to identify fine sub-neuronal structures and a high imaging speed, which is a critical concern in large-scale organ mapping.

Comparisons with Gaussian sheet, confocal and Two-Photon-Excitation microscopy

As confocal microscopy remains the workhorse for 3D cellular imaging and the Gaussian light-sheet method is the standard for light-sheet microscopy, we compared both techniques with various modes of Bessel beam plane illumination. Image slices in the *x-z* plane from dendrites of Thy1-GFP-M mouse brain demonstrating comparative axial resolutions were acquired using a selective plane illumination microscope (SPIM, 0.02 NA illumination, 12.6×/0.5 detection objective), a point-scanning confocal microscope (Nikon Ni-E, CFI LWD 16×/0.8W objective), a two-photon-excitation (TPE) microscope (Nikon Ni-E, CFI LWD 16×/0.8W objective), the synchronized Bessel sheet mode (0.28 NA illumination, 12.6×/0.5 detection objective), the synchronized Bessel sheet mode with deconvolution (a parallel iterative deconvolution method in an ImageJ plugin) and the CACS-enabled Bessel sheet mode (**Fig. 2a-f**). The thick Gaussian sheet covering the full imaging FOV (~1 mm) gave insufficient axial resolution (FWHM ~10 μm, **Fig. 2a**), which was obviously poorer than that of the other methods. With the confocal and TPE microscopes, the anisotropic PSFs in the epifluorescence mode influenced the visualization of the dendrite fibers in the longitudinal direction (**Fig. 2b, c**). In contrast, the

three Bessel sheet modes all demonstrated a clear reduction in out-of-focus haze, as well as high axial resolution superior to the Gaussian sheet, confocal and TPE methods (**Fig. 2a-f**). It is not surprising that deconvolution using a bead-measured synchronized Bessel mode's PSF did not alter the image quality much, except for slightly increasing the contrast. The CACS substantially recovered the ultrastructure of the dendrites, which remained unresolvable in the raw image (**Fig. 2f, i**). while the fidelity was shown to be sufficiently high (**Fig. 2j, k**). The bead measurements and line cuts through individual dendrite fibers (**Fig. 2a-f**) made by each method further reveal the narrower axial and lateral FWHMs of the CS Bessel sheet modes in comparison with the regular Bessel sheet. The experimentally measured axial FWHMs were 10, 1.29, 0.72, 4.375 and 5 μm for Gaussian light-sheet, synchronized Bessel sheet, CS Bessel sheet, confocal and TPE methods, respectively (**Fig. 2l**). The corresponding lateral values were 1.29, 1.29, 0.67, 0.83 and 0.875 μm. Aside from the resolution improvement, the CACS procedure also significantly improved the SNR, as shown in **Supplementary Fig. 11**.

For large-scale imaging, which often encompasses data from hundreds of gigavoxels, the achievable resolution needs to be carefully balanced with the imaging time, because of the limited space bandwidth product (SPB) of the system[28]. The achievement of sufficiently precise measurements in a reasonably short acquisition time with a low photo-bleaching rate thereby poses a big challenge. For example, confocal and TPE microscopes can three-dimensionally image a sample at fairly high resolution (3 μm^3), but do so at the cost of low speed due to the point scanning detection (4.2×10^4 $\mu m^3/s$), and noticeable phototoxicity caused by the epi-illumination mode. In contrast, Gaussian or Bessel sheet modes with in-plane excitation and camera-based detection can image the sample at video rate speed and with lower photo-bleaching. The CACS-enabled Bessel sheet mode further improves the volumetric resolution by over 15 times, while maintaining the same acquisition speed and bleaching rate, thereby resulting in a higher throughput.

We compared the degree of photo bleaching of the five imaging methods by repeatedly imaging the cortex area of a Thy1-GFP-M mouse brain 30 times (**Supplementary Fig. 12**). After normalizing for differences in SNR (see Methods), we calculated the averaged signal intensity of each volume for each method, and plotted their variations in **Fig. 2m**. After 30

cycles of imaging of the same volume, approximately 95%, 80%, 40%, and 30% of the fluorophores were preserved by the Gaussian sheet, Bessel sheet, TPE, and confocal methods, respectively. In **Fig. 2n** and **Supplementary Table 1**, we further rate the overall imaging performance of confocal, TPE, Gaussian sheet, Bessel sheet, and CACS Bessel sheet methods by comparing their volumetric resolutions, acquisition speeds, and photo-bleaching rates. The CACS-enabled Bessel sheet method boosted imaging throughput while achieving isotropic 3D resolution of ~0.7 μm across a 1 × 1 × 1 mm FOV in ~65 seconds (Methods, **Supplementary Table 1**). Under the lower magnification of 3.2× used for whole-brain imaging, the CACS Bessel sheet mode yielded an isotropic resolution of ~1.6 μm at a high acquisition rate of ~1 $mm^3\ s^{-1}$. As shown in the data projected to a resolution-speed plane, the CACS Bessel sheet mode breaks the SPB limitation defined by the dashed resolution-speed curve. Thus, it can be considered to be a tool facilitating the combination of a large FOV with isotropic high-resolution, which is difficult to meet using previous methods.

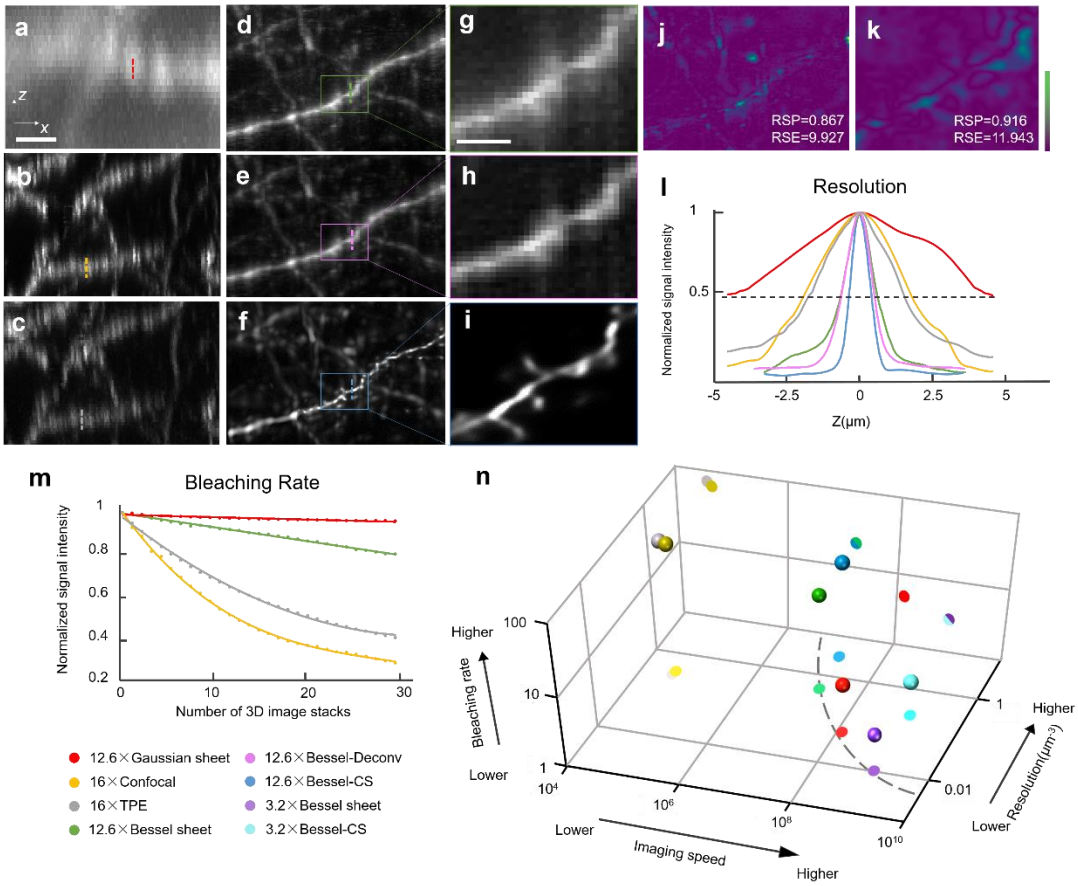

Fig. 2 | Comparisons of CACS Bessel sheet modes to confocal, TPE, and SPIM. a-f, Comparative image slices in an *x-z* plane through GFP-labelled neurons in a cleared mouse cortex by: Gaussian sheet

(**a**, 0.02 NA illumination + 12.6×/0.5 detection); point-scanning confocal microscopy (**b**, 16×/0.8); two-photon excitation microscopy (**c**, 16×/0.8); Bessel light-sheet illumination (**d**, 0.28 NA illumination + 12.6×/0.5 detection); Deconvolved Bessel sheet (**e**); CACS Bessel sheet (**f**). Scale bars, 20 μm (inset, 5 μm). **g-i**, Magnified views of a dendrite in (**d-f**), with CACS result successfully resolving the sub-micron spines. **j**, **k**, Error map between CACS and conventional Bessel sheet result, indicating the fidelity after resolution improvement. (**l**) Linecuts (as shown in insets in **a-f**) for each method, with 50% intensity level shown for estimation of the FWHM. **m**, Bleaching rates obtained from repeated 3D imaging (30 times) of neurons in mouse cortex, normalized to account for differences in SNR. **n**, 3D plot comparing the acquisition speed, bleaching rate and volumetric resolution of 8 imaging modes indicated by different colors. The dashed line that connects the data points of 3.2× Bessel sheet, 12.6× Gaussian sheet and 12.6× Bessel sheet projected in speed-resolution plane represents the throughput limit in conventional light-sheet microscopes.

Rapid 3D isotropic imaging of mouse brain at various scales

The improved axial resolution at various scales obtained from the tunable Bessel plane illumination and the expanded SPB made possible by the CACS computation enables brain (or other organs) imaging with isotropic resolution and very high throughput. For example, under the 1.26× dual-side Bessel sheet mode, over 2000 large-FOV image slices can be acquired in two views in ~60 seconds, image slices that can be computationally fused to provide an image of the whole brain[2] (Methods). We here demonstrate the fast screening of four optically-cleared mouse brains (Tg: Thy1-GFP-M, **Fig. 3b**) imaged at a throughput of one brain min^{-1} and ~10 μm isotropic resolution. By obtaining the coarse 3D structures of the whole brains using the widest Bessel sheet (**Fig. 3b**), the transverse (*x*-*y*), coronal (*x*-*z*), and sagittal (*y*-*z*) views could be extracted from the reconstructed brains to quickly identify brain regions where desired signals were present (**Fig. 3c**). Then, higher-resolution imaging of any region of interest was possible using the 12.6× Bessel sheet mode. For example, we imaged three ~1 mm^3 regions of interest (ROIs) in the cortex, hippocampus, and cerebellum of brain number 2 (**Fig. 3b**) at an imaging speed of ~0.017 mm^3 s^{-1} and an isotropic resolution of ~1.3 μm (0.5 μm voxel). Vignette high-resolution views of these volumes are shown in **Fig. 3d-f**, detailing the various neuron morphologies across the brain. Besides the identification of different types of neuron cell bodies (e.g., pyramid neurons in **Fig. 3e**, and astrocytes in **Fig. 3f**), nerve fibers such as densely packed apical dendrites (**Fig. 3d**) were also clearly resolved in three dimensions. If finer neuronal sub-structures are of interest, the CACS described above can be readily integrated to super-resolve such structures, for example, the spines shown in **Figs. 1f** and **2i**.

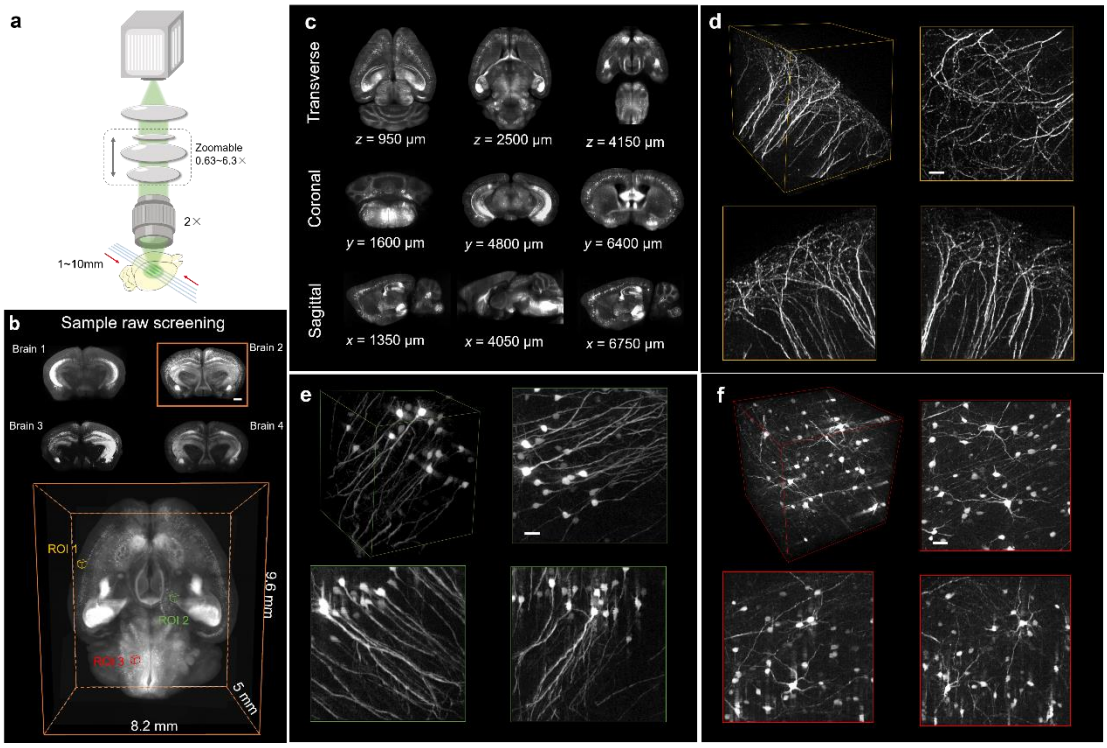

Fig. 3 | Scalable isotropic imaging of neurons in mouse brain. a, Dual-side, tunable Bessel sheet illumination combined with zoomable detection FOV from 1.26× (1.1 cm) to 12.6× (1.1 mm). **b**, Reconstructed coronal planes of four mouse brains that are rapidly screened using raw 1.26× Bessel sheet mode. Each brain was imaged under 2 views for generating a multi-view-fused 3D reconstruction that contains 1100 image planes. The right column shows volume rendering of a whole brain (No.2) selected, owing to its best signal distribution among 4 candidates. **c**, MIPs in transverse (*x*-*y*; top), coronal (*x*-*z*; middle), and sagittal (*y*-*z*; bottom) planes of the No.2 whole brain, showing the overall signal distributions. **d-f**, Three ~1 mm^3 ROIs in cortex (yellow), hippocampus (green), and cerebellum (red) regions, selected from the coarse 1.26× reconstruction, and further imaged by 12.6× Bessel sheet mode, to reveal the various neuron types/structures (dense dendrites in **d**, pyramid neurons in **e**, astrocytes in **f**) at subcellular isotropic resolution.

3D imaging of single neurons in the whole brain at a time scale of minutes

A key advantage of whole brain mapping is that the high-resolution visualization across a large volume permits the investigation of complicated neural circuits, such as neuron phenotyping in various functional regions and the trajectories of long-distance neuronal projections. These pose challenges for imaging systems with limited optical throughput. For example, the SBP of the raw Bessel sheet is sufficient for either fast low-resolution screening of the whole brain (1.26×) or high-resolution observation of small ROIs (12.6×). Therefore, high-resolution neuron mapping across the entire brain requires the combination of a 12.6× Bessel sheet with

mechanical stitching to artificially increase the system SBP. However, the need for hundreds of stitching operations limits the acquisition of whole-brain imaging to the timescale required to collect one million frames at the desired isotropic resolution.

Therefore, to quickly image neurons exhibiting long-distance details across the whole brain, a CACS Bessel sheet is necessary. A cleared mouse brain (~10 × 8.5 × 5 mm) was first imaged using the 3.2× Bessel sheet mode (FOV 4.2 mm, **Fig. 4a1**) under two views, each containing six stacks (**Fig. 4a2**). Then, tile stitching[36] for each view (**Fig. 4b1, 2**) followed by a two-view fusion[37] was applied to obtain the 3D image of complete brain (**Fig. 4a2, 4b3**; 2 μm voxel). CACS was applied at the last step (**Fig. 4a3**) to generate a final output (0.5 μm voxel) with resolved nerve details comparable to those obtained with the 12.6× Bessel sheet (**Fig. 4b4, c, Supplementary Fig. 7**). The 15-minute rapid acquisition combined with parallel computation using multiple GPUs permits the reconstruction of a digital brain with isotropic subcellular-resolution over a 400 mm^3 volume (Methods, **Supplementary Table 2**). This allows brain segmentations and accurate quantifications to be performed at a system level (**Fig. 4a4**). For example, we precisely traced interregional neuron projections, which are important for understanding the functionality of the brain. Compared with the raw image, the CACS visualized more nerve fibers (**Fig. 4c**), thus enabling neuronal trajectories with abundant details to be presented in three dimensions (**Fig. 4d**). By referring to the standard mouse brain atlas (Allen Brain Institute)[3,38], anatomical information was annotated onto the CACS Bessel brain Atlas, and the trajectories of four long-distance (LD) projection neurons were traced and registered to the annotations, revealing how their pathways were broadcast across the anatomical regions (Methods, **Supplementary Fig. 13, Video 1**). With isotropic submicron resolution, 13 densely-packed Pyramidal neurons could be also be identified and traced through the entire cortex to the striatum (~2 × 2 × 2 mm^3), as shown in **Supplementary Fig. 13**. This quantitative analysis was implemented in a Thy1-GFP-M mouse with massive numbers of neurons being labeled, and this procedure would be even more efficient if the brain was more specifically labeled (e.g., by virus tracer).

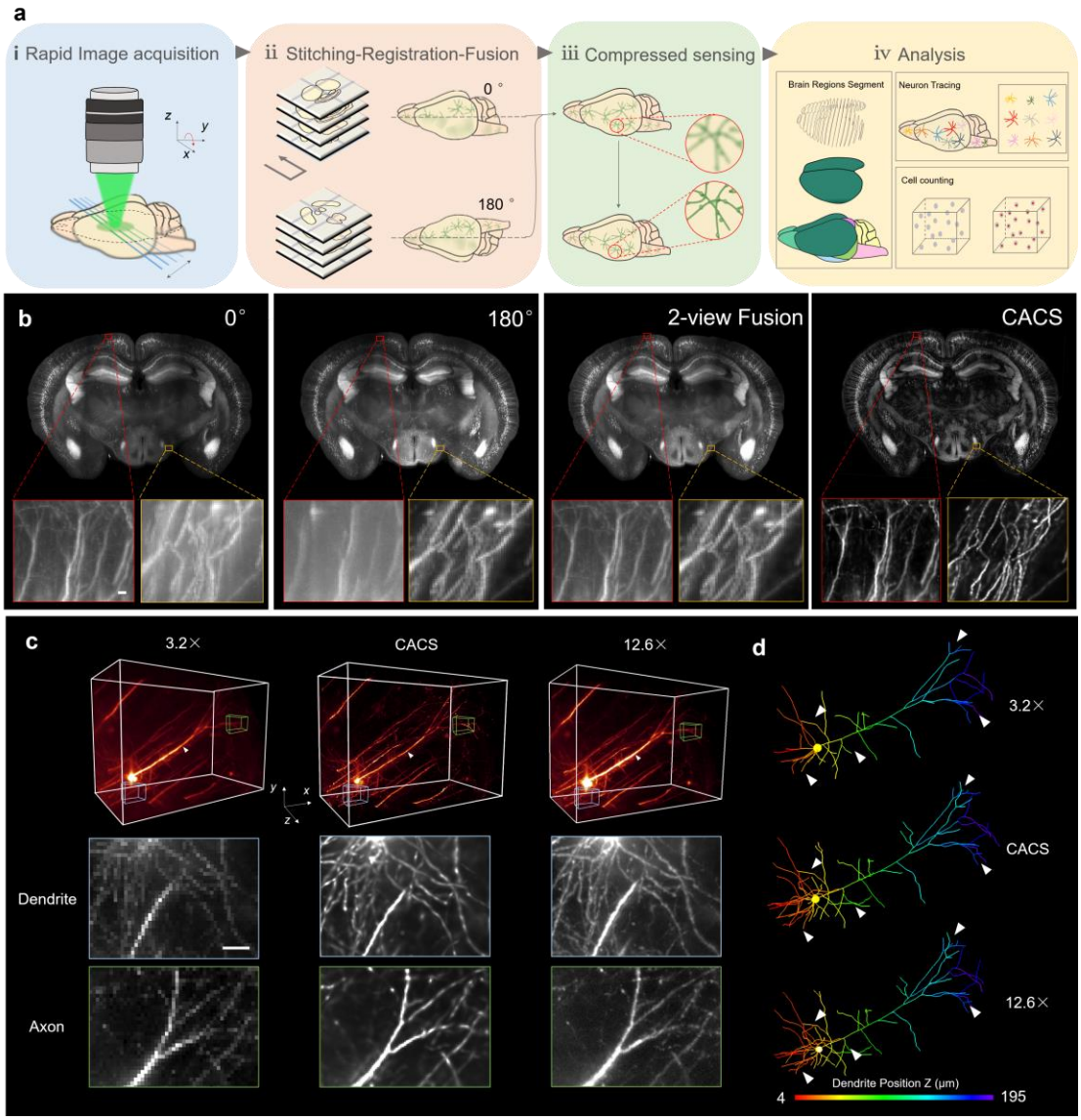

Fig. 4 | Whole-brain mapping pipeline. a, Flow chart of whole-brain data acquisition and processing, which includes: **i**, rapid image acquisition by 3.2× Bessel sheet, with total 12 tiles under 2 views acquired in ~15 minutes. **ii**, tile stitching for each view followed by 2-view weighted fusion, to reconstruct a scattering-reduced whole brain at low resolution (2 μm voxel). **iii**, CACS computation to recover a digital whole brain with improved resolution (0.5 μm voxel) and SNR. **iv**, quantitative analysis, such as brain region segmentation, neuron tracing and cell counting, based on high-quality whole brain reconstruction. **b**, A coronal plane (*x*-*z*, 100-μm thickness) in whole brain reconstructed by 0°, 180° single view Bessel sheet, 2-view fusion and CACS computation. The magnified views of two small regions selected from z = 100 and z = 4500 μm depth further show the effect of 2-view fusion and CACS. **c**, 3D volumes reconstructed by raw 3.2× (left column), 3.2× CACS (middle column), and 12.6× (right column) Bessel sheet modes, with magnified views of dendrites (middle row) and axons (bottom row) showing the resolving power of each mode. **d**, Improvement for single neuron tracing brought by CACS. The same pyramidal neuron imaged by three modes was segmented and traced using Imaris. The results clearly show the improvement of segmentation accuracy (white arrows) brought by CACS. Scale bar, 10 μm.

3D imaging and cell counting in half of a mouse brain

In addition to the tracing of neuronal projections, the cyto-structures at different brain sub-regions were also explored using CACS Bessel sheet imaging (**Fig. 5**). In order to obtain numbers of cell in different sub-regions with the irregular and diversified morphologies of cells, we labelled nuclei with propidium iodide (PI), an organic small molecule staining DNA. Almost all cell nuclei including motor axons and retinal ganglion cells were stained, causing very dense fluorescing (**Fig. 5a**). Raw 3D images of the nuclei in half brain quickly obtained by 2× CACS sheet mode (**Fig. 5a**; in ~4 minutes), signals remained highly overlapped and undistinguishable (**Fig. 5b1**). Identically, CACS offered a 4× resolution enhancement in each dimension to recover images with resolution even better than 8× Bessel sheet, to discern single nuclei (**Fig. 5b2**). The vignette high-resolution views show that cell counting based on the CACS was as accurate as that using an 8× Bessel sheet (**Fig. 5c2, 3**). After anatomical annotation was applied by registering the image volume to the aforementioned Allen brain atlas (ABA), the labelled cells could be properly segmented (**Fig. 5d-g**), with each individual cell being assigned an anatomical identity, such as isocortex, hippocampus formation, olfactory area, cerebral nuclei, cortical subplate, thalamus, hypothalamus, midbrain, hindbrain, or cerebellum, as shown in **Fig. 5h, i**. We did not observe morphology- or size-dependent errors in cell detection in different regions. By registering and annotating the detected cells to anatomical areas in the CACS Bessel Atlas, cell number and density information for these brain regions was quantified (**Supplementary Fig. 14, 15 and Video 2**). As shown in **Fig. 5j**, the total cell number in the half brain was ~3.5×10^7, and the average density was ~2.4×10^5 cells per mm^3. Amongst the primary brain regions, the Isocortex showed the highest number of cells at 8.6×10^6, which compares with 2.3×10^6, 7.3×10^6, 5.3×10^5, 3.6×10^6, 2.4×10^6, 1.4×10^6, 2.8×10^6, 1.3×10^6 and 3.7×10^6 cells in the Olfactory area (OLF), Cerebellum (CB), Cortical subplate (CTXsp), Cerebral nuclei (CNU), Hippocampal formation (HPF), Hypothalamus (HY), Midbrain (MB), Thalamus (TH), and Hindbrain (HB), respectively. The cerebellum had the highest cell density of ~4×10^5 cells per mm^3, compared with 2.5×10^5, 2.4×10^5, 2.3×10^5, 2.1×10^5, 2.1×10^5, 2.6×10^5, 2.2×10^5, 2.0×10^5 and 1.7×10^5 in the other regions listed above. Although the current results were obtained using a PI-stained half brain, in which ~50% of all motor axons and retinal ganglion cells were counted, our results are consistent with previously reported work[2].

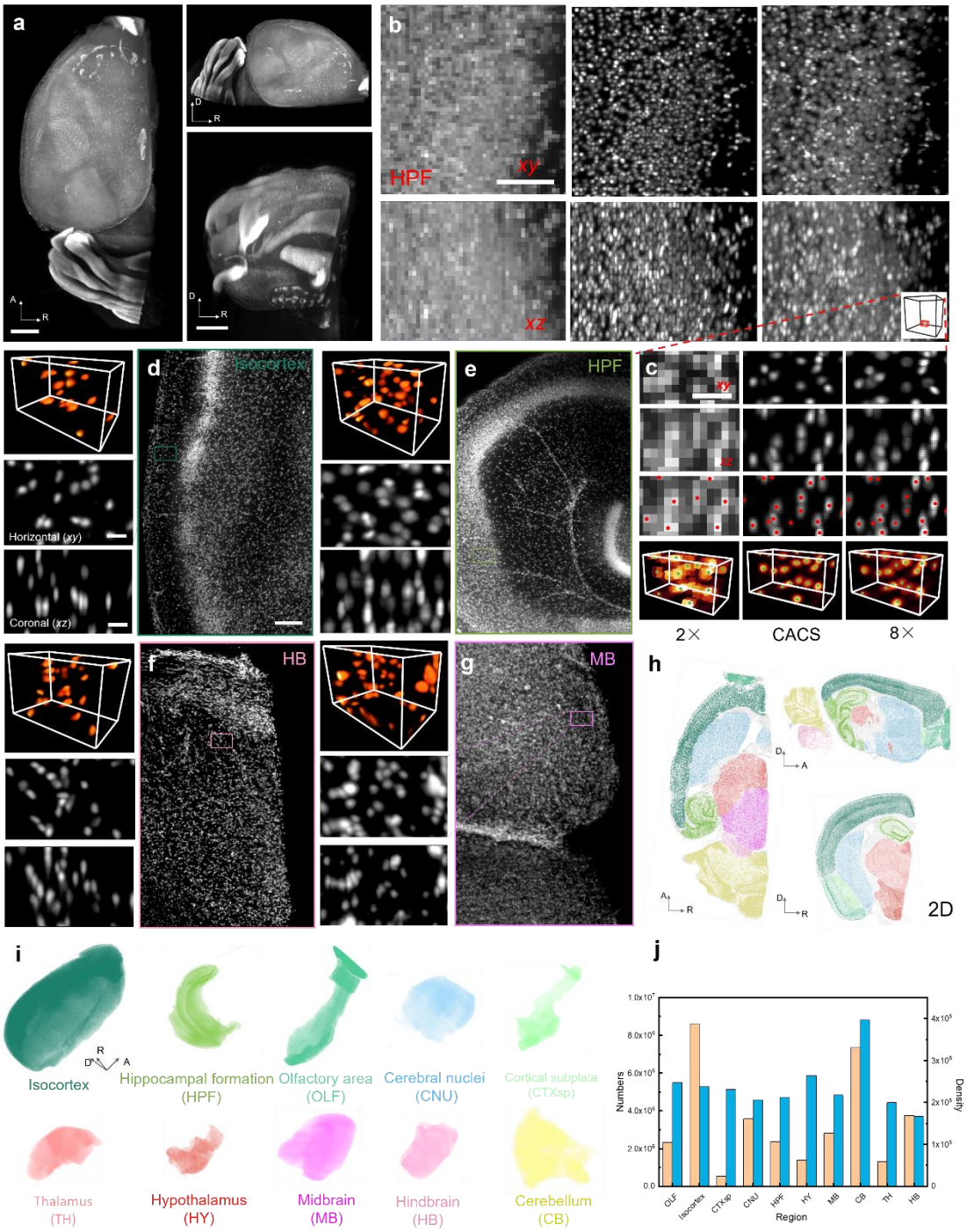

Fig. 5 | Cell counting of propidium iodide (PI)-labelled half mouse brain. a, Coronal view, transverse view and sagittal view of PI-labelled half mouse brain image by 2× CACS Bessel sheet. Scale bar, 1 mm. **b**, A selected ROI in HPF, resolved by 2× Bessel sheet (left column), 2× CACS Bessel sheet (middle column), and 8× Bessel sheet (right column). **c**, Magnified views of a small volume (red box) in **b**, showing the different accuracy of nuclei based identification base on three types of images. Scale bar, 20 μm in **b** and 10 μm in **c**. **d-g**, 3D visualization of four high-resolution ROIs from Isocortex, HPF, HB and MB regions in the reconstructed half brain. Scale bar, 50 μm in large box and 10 μm in small box. The results clearly show single-cell resolution in three dimensions, which is sufficient for cell counting. **h**, 10 manually segmented brain regions in the half brain, shown in transverse, coronal, and sagittal views. **i**, 3D visualization of the 10 sub-regions indicated by different colors. **j**, Calculated nuclei number and

density of each sub-region in half brain.

Dual-color 3D imaging and quantitative analysis of neuro-muscular junctions

We further demonstrated dual-color CACS Bessel sheet imaging of motor endplate (MEP, α-BTX) and peripheral nerves (Thy1-YFP) in mouse muscle. The overall spatial distribution of MEPs in the muscle tissue and the detailed neuromuscular junction (NMJ) occupancy defined as the volume ratio of the underlying postsynaptic MEPs (red) occupied by presynaptic vesicles (green), were both visualized and analyzed using the large-scale high-resolution CACS Bessel imaging. We rapidly imaged two total gastrocnemius muscles and two total tibialis anterior muscles in ~20 minutes (**Fig. 6a-d**), with segmentation of their MEPs and nerves (insets in **a-d**). The number of MEPs and their density in the tissue of each muscle were quantified from the resulting whole-tissue imaging (**Fig. 6e**). We found that although the total MEP number varied in each muscle, their density remained relatively close. Magnified views of the NMJs (2 ROIs in **6a**) are shown in **Fig. 6f,** with comparable views of the 12.6× and 3.2× CACS-delivered results (middle, **Fig. 6f**), which show quality as high as the views obtained at 12.6× (right, **Fig. 6f**), allowing the resolving of fine neuromuscular structures in single NMJs. Therefore, our technique permitted the accurate measurement of presynaptic and postsynaptic structural volumes in single NMJs and the calculation of NMJ occupancy (**Fig. 6g**), measurements that are not possible using conventional 3.2× Bessel results because of insufficient spatial resolution (left, **Fig. 6f**). These complete visualization and quantitative analyses enabled by CACS Bessel sheet imaging indicate both the movement capability of muscle tissues at a macro scale, and the delivery efficiency of neurotransmitters at nerve endings on a micro-scale, thereby potentially benefiting the comprehensive understanding of neuromuscular functional activities and improving the diagnosis and development of therapy for related diseases[39,40].

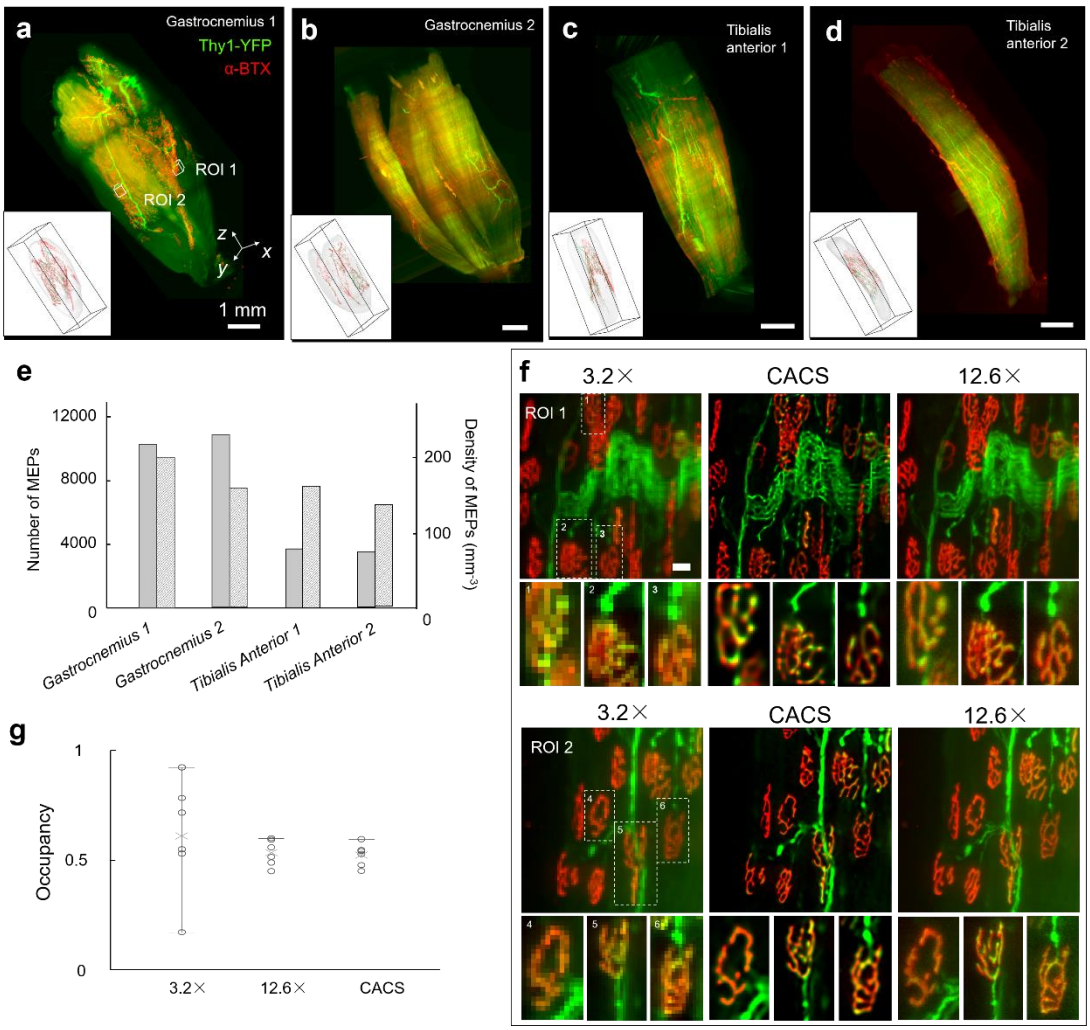

Fig. 6 | Dual-color CACS imaging and quantitative analysis of neuromuscular junctions in mouse Gastrocnemius and Tibialis anterior. a-d, Dual-color, 3D visualization of Gastrocnemius and Tibialis anteriors, showing both the presynaptic terminal bouton (green, Thy1-YFP) and postsynaptic acetylcholine receptors (red, α-BTX). Insets show segmentation of presynaptic terminal and MEPs. **e**, Macro-scale quantitative analysis of MEP, including total numbers and densities of MEPs, in two types of muscles. **f**, Comparison of two ROIs in **a**, by 3.2× (left column), 3.2× CACS (middle column) and 12.6× Bessel sheet (right column). Magnified views of six small areas (white boxes, 1, 2, 3 for ROI1 and 4, 5, 6 for ROI2) further demonstrate the structural information of single NMJs. Scale bar, 10 μm. **g**, Neuromuscular junction (NMJ) occupancy calculated based on abovementioned 3.2×, 3.2× CACS and 12.6× Bessel sheet images that show different level of resolution. The result from 3.2× image shows an unacceptably large error range, owing to the ambiguous cellular resolution. Here NMJ occupancy was calculated as (presynaptic volume/postsynaptic volume) *100.

Discussion

In summary, the marriage of the CACS strategy with long-range Bessel plane illumination provides 3D isotropic resolution down to ~700 nm, and the ability to quickly acquire 3D images from millimeter-to-centimeter sized brains in seconds to minutes, at a scalable throughput of

up to 8 gigavoxels per second. The readily-tunable Bessel sheet setup combined with zoomable macro-view detection is well suited for the isotropic 3D imaging of not only mouse brain, but also other entire organs/organisms at variable scales. Highly inclined LSM has been used for the 3D anatomical mapping of thick organs where autofluorescence and out-of-focus excitation would otherwise be prohibitive under wide-field illumination. With the thinner light-sheets of the Bessel beam, the effective FOV would be less compromised, and axial resolution would be further improved. The introduction of dual-side illumination and dual-view detection would further reduce light depletion in thick tissue and permit the complete interrogation of entire organs. As currently configured, the key step to maintaining thin and wide Bessel plane illumination under a large FOV is to synchronize the scanned beam with the confocal electronic slit of the camera, to eliminate excitation from the side-lobes. This could possibly be improved by direct generation of a side-lobe-reduced Bessel sheet using recent masking techniques[41]. At the other extreme, the possible introduction of two photon excitation may be furthermore suited for improved depth penetration when imaging more scattering samples.

Despite the use of plane illumination, current microscopes have throughput limited to megavoxels per second. This causes issues in 3D anatomical mapping, in which trillion-voxel data is frequently required. Therefore, the long-time acquisition required for mechanical image stitching prevents a variety of histological, pathological, and neuroanatomical research being implemented on a large scale. Our CACS procedure uses a single image stack to three-dimensionally improve the contrast and resolution limited by the pixilation and numerical aperture, computationally transforming our Bessel microscope into a gigavoxel-throughput-boosted imager that can achieve isotropic 3D super-resolution imaging of mesoscale samples without the pain of a long acquisition lasting for hours to days. Considering that signal characteristics such as sparsity and degree of disorder vary drastically in large specimens, it is difficult for regular CS computation to process the signals appropriately, because it is uncertain what regularization factor should be applied. Our introduction of a content-aware feedback strategy can reasonably extract the signal characteristics and thereby calculate the optimal regularization parameter for each image block automatically, allowing recovery of signals on a large scale with minimal artifacts, as well as obvious resolution improvement, which is unmet

by conventional CS (**Supplementary Fig. 9**). Our 3D CACS computation is unsupervised, without the need for prior knowledge from a higher resolution database, and is highly parallelized for GPU acceleration. It should be noted that CS processing is efficient for the recovery of under-sampled signals, a condition particularly satisfied in our low-magnification large-FOV imaging setup. Moreover, although compressed sensing is known to have certain limitations for processing signals containing complicated structural information[42,43], its effect on line-like neurons and point-like nuclei was significantly improved after the content-aware adaption to the signal characteristics involved. We expect our method to potentially bring new insights for computational imaging techniques, so that we can keep pushing the optical throughput limit to extract ever more spatiotemporal information from biological specimens. We also believe that combinations with other computational techniques, such as neural network-enabled data training, could further increase the ability of our method to achieve more robust and versatile recovery of various complicated signals in different types of specimens.

Methods

Zoomable Bessel plane illumination microscopy setup. The optical setups of zoomable Bessel plane illumination microscope were detailed in **Supplementary Figs. 1, 2**. To maintain sufficient laser intensity at large scale, we used a large apex axicon (176e, AX252-A, Thorlabs) instead of mask to create annular beam at a plane conjugate to both the galvanometer and the rear pupil of the excitation objective. For the Bessel beam, its axial extent of central maximum (beam thickness) and diffraction distance (beam length) are proportional to the magnification of the illumination objective and its square, respectively. Thus, a pair of long working distance objectives (Mitutoyo, 2×/0.055, or 5×/0.14, or 10×/0.28) were used to generate dual-side illuminating Bessel beam with diffraction range from 1 to 25 mm and thickness 1 to 5 μm adapted to the zoomable detection FOV of 10 to 1 mm as well as variable lateral resolution of ~10 to 1 μm by macro-view microscope (MVX10, 1.26× to 12.6×, Olympus). To achieve side-lobe free imaging based on electronic confocal slit, we formed a linear array which contains 2-4 rows of active pixels sweeping at the sensor plane along *y* direction, and tightly synchronized its movement with the central maximum of scanned Bessel beam. During image acquisition, the 2D galvo mirror (GVS012, Thorlabs) that scans the Bessel beam into plane, the sCMOS

camera (Hamamatsu ORCA-Flash4.0 V2) that continuous records the fluorescence images at high speed up to 50 frames per second, the motorized *xyz* stage (Z825B, Thorlabs combined with SST59D3306, Huatian) that moves the sample in three dimensions, and the motorized flip mirror that switches the illumination between dual beams, were all controlled by analog signals generated by a data acquisition device (PCIe-6259, National Instruments). A LabVIEW (National Instruments) program was developed to synchronize these parts, to automatically realize the line-synchronized scanning, *z*-scanning and tile-stitching in order. For the imaging of an entire organ, the sample was flipped 180 degrees up-side down to be imaged twice. Due to the corrosive BABB immersion solution, a micro-motor was sealed inside a chemical-resistant resin box and attached to the sample holder to fulfill the precise rotation (**Supplementary Fig. 2**). The two-view images were then registered and fused using multi-view fusion method[37].

CACS computation procedure. If the signals are not dense and incoherent at the same time, CS allows the recovery of them from incomplete measurement, which is our case in large-FOV Bessel sheet imaging. To correlate the high-resolution image to be recovered with the real measurement, we first used a 3D Gaussian-Bessel function as PSF to characterize the unit response of the Bessel sheet system. The lateral and axial extents of the PSF are determined by a variety of imaging parameters, such as NA of illumination and detection objectives, and camera's spatial sampling rate. Then a measurement matrix A could be generated by Fourier transformation of the synthetic PSF. Here A represents the signal degradation operation including the optical blurring by system optics and down-sampling by the camera digitalization in Fourier space, transforming the high-resolution target into low-resolution measurement. Then the Fourier expression of high-resolution image x can be recovered from the Fourier expression of low-resolution measurement y by iteratively solving following equation in Fourier domain using a steepest descent method:

$$X_{n+1} - X_n = \|AX_n - Y\|_2^2 \tag{2}$$

The recovered image can be finally obtained via transforming the solved x back into spatial domain. As we have known, compressed sensing could show very different effects on signals with different labelling density, which is particularly common to large samples. An L1-

normalization term was thus introduced in our method to regularize the equation as following:

$$\|X_{n+1}\|_1 = \|AX_n - Y\|_2^2 + \lambda\|X_n\|_1 \quad (3)$$

Here the weighting factor λ substantially balances the image results from more like the original measurement to more like the CS recovery. The value of λ is calculated by the multiply of α and β, where α is an index indicating the signal density of input image (**Supplementary Note 3**), and β is inversely proportional to the entropy of the input image (**Supplementary Note 3**). Therefore, the choice of λ is highly adapted to the signals characteristics which could vary a lot at large scale, our content-aware processing procedure divides the raw image, e.g, half brain image with dimension 10 mm × 4 mm × 5 mm, into a series of small volumes, e.g., blocks with 100 × 100 × 100 pixels in which the signals can be considered as uniformly distributed, and then calculates the regularization factor for each volume to obtain the optimal CS result x_i. Multiple x_i are transformed back to high-resolution image blocks, which would be stitched into final output. It should be noted that the CACS computation can be highly parallelized by using GPU acceleration.

Whole-brain imaging procedure. Lowest 1.26× detection combined with dual-side 1 cm-Bessel sheet illumination (5 μm thick) was first used to roughly screen the brains. Under this mode, stitching is not required and the resolution is not necessarily high, at ~10 μm. The overall signal distributions of every brain could be readily obtained via rapid data acquisition in a few seconds followed by a registration-and-fusion of 2 views in a few minutes. As for high-resolution mapping of whole brain to enable quantitative analysis, the choice of tile stitching over 100 times under 12.6× is not only very time consuming, estimated with over 10 hours, and brings substantial photo-bleaching. Instead, we imaged the whole brain at lower 3.2× Bessel sheet mode and used CACS to computationally improve the compromised resolution. With 4 by 4 mm FOV under 3.2×, we sequentially obtained 6 volumes of the different regions of the brain with each one containing 1500 frames for 3 mm *z*-depth (2 μm step-size), and stitched them into a whole 3D image. Then, two views of stitched images were iteratively registered for reconstructing a whole brain with exhibiting complete structural information while presenting spatial resolution ~4 μm (2 μm voxel), which remains insufficient for single-cell analysis. Nevertheless, CACS was applied with dividing the whole brain into thousands of blocks,

processing them using 4 GPUs (RTX2080ti) in parallel. Finally, a 3 trillion-voxel image was created (0.5 μm voxel) with acquisition time ~15 minutes which is compared to tens of hours by other methods[1], and computation time ~50 hours which is estimated similar with the time consumption for stitching and fusion under 12.6×.

It should be noted that the combination of Bessel sheet with CACS is very flexible, providing throughput improvement for zoomable imaging from 1.26× to 12.6×. It is also easy to modify the LabVIEW program to conduct imaging under different modes/magnifications. Thus, it's beyond the imaging of brain we demonstrate, being widely suited for anatomical imaging of various large samples, such as mouse muscles shown in **Fig. 6**.

Sample preparation. UDISCO clearing method was used to clarify the dissected wild-type mouse brain with cell nuclei stained by PI dye, neuron-labelled mouse brain blocks (Tg: Thy1-GFP-M). FDISCO clearing method[44] was used to clarify the neuron-labelled mouse muscles (Tg: Thy1-YFP-16) with α-BTX tagging the motor endplate. PEGASOS clearing method[45] was used to clear the Thy1-GFP-M whole mouse brain, The cleared organ samples (**Fig. 6**) were harden and thus could be firmly mounted onto our customized holders (**Supplementary Fig. 2**). The BABB-D4 for UDISCO, DBE for FDISCO or BB-PEG for PEGASOS immersion liquid was filled in the sample chamber for refractive index-matched imaging with least aberration. For measuring the system's point spread function, fluorescent beads (Lumisphere, 1%w/v, 0.5 μm, Polystyrene) were embedded into a specifically formulated resin (DER332, DER736, IPDA, 12: 3.8: 2.7), the refractive index of which was equal to BABB-D4, to form a rigid sample that can be clamped by the holder and imaged in the chamber.

Whole-brain visualization and registration to ABA. The processed brain atlas was interactively visualized using Imaris software (Bitplane, USA). Since the Allen Brain Atlas was reconstituted from a series of coronal-slice images, we also rotated our reconstructed image and down-sampled it, to register it with anatomically-annotated ABA based on the coronal slices. Automatic Elastix registration was applied first to roughly align the brain. Then a manual adjustment was followed to improve the accuracy.

Neuron tracing. The whole brain data was down-sampled 2 times and segmented manually

using the commercial Imaris software. With registering our brain to ABA, we obtained the anatomical annotation for all the segmented areas. The Autopath Mode of the Filament module was applied to trace long-distance neurons. We first assigned one point on a long-distance neuron to initiate the tracing. Then, Imaris automatically calculated the pathway in accordance with image data, reconstructed the 3D morphology and linked it with the previous part. This automatic procedure would repeat several times until the whole neuron, which could also be recognized by human's eye, was reconstructed.

Cell counting. The Spots module and Surface module of commercial Imaris software was used to count cells in various anatomical regions of CACS-reconstructed half brain (full resolution, ~400 gigavoxels). We first separated several primary brain regions into different channels in Surface module. Then automatic creation in Spots module was applied to count cells number for each single channel which represents a encephalic region. To achieve accurate counting, the essential parts were the appropriate estimate of cell bodies' diameter and filtration of the chosen cells by tuning the quality parameters. This automatic counting procedure was also aided by human's crosscheck, which herein severed as golden standard.

Acknowledgements

We thank Shangbang Gao, Luoying Zhang, Haohong Li, Man Jiang, Bo Xiong for discussions and comments on the manuscript, Yunyun Han for the discussion on the imaging and brain visualization. This work was supported by the National Key R&D program of China (2017YFA0700501, D.Z. and P.F.), the National Natural Science Foundation of China (21874052 for P.F., 61860206009 for D.Z.), the Innovation Fund of WNLO (P.F. and D.Z.) and the Junior Thousand Talents Program of China (P.F.).

References

1 Osten, P. & Margrie, T. W. Mapping brain circuitry with a light microscope. *Nature Methods* **10**, 515-523 (2013).

2 Murakami, T. C. *et al.* A three-dimensional single-cell-resolution whole-brain atlas using CUBIC-X expansion microscopy and tissue clearing. *Nature Neuroscience* **21** (2018).

3 Dong, H. W. The Allen reference atlas: A digital color brain atlas of the C57Bl/6J male mouse. *Quarterly Review of Biology* (2008).

4 Lichtman, J. W. & Denk, W. The big and the small: challenges of imaging the brain's circuits. *Science* **334**, 618-623 (2011).

5 Miyamichi, K. *et al.* Cortical representations of olfactory input by trans-synaptic tracing. *Nature* **472**, 191-196 (2011).

6 Webb, R. H. Confocal optical microscopy. *Rep.prog.phys* **59**, 427 (1996).

7 Madisen, L. *et al.* A robust and high-throughput Cre reporting and characterization system for the whole mouse brain. *Nature Neuroscience* **13**, 133-140 (2010).

8 Silvestri, L., Bria, A., Sacconi, L., Iannello, G. & Pavone, F. S. Confocal light sheet microscopy: micron-scale neuroanatomy of the entire mouse brain. *Optics Express* **20**, 20582-20598 (2012).

9 Frasconi, P. *et al.* Large-scale automated identification of mouse brain cells in confocal light sheet microscopy images. *Bioinformatics* **30**, i587 (2014).

10 Helmchen, F. & Denk, W. Deep tissue two-photon microscopy. *Nature Methods* **2**, 932 (2005).

11 Timothy, R. *et al.* Serial two-photon tomography: an automated method forex-vivomouse brain imaging. *Nature Methods* **9**, 255-258 (2012).

12 Huisken, J., Swoger, J., Bene, F. D., Wittbrodt, J. & Stelzer, E. H. K. Optical Sectioning Deep Inside Live Embryos by Selective Plane Illumination Microscopy. *Science* **305**, 1007-1009 (2004).

13 Dodt, H. U. *et al.* Ultramicroscopy: three-dimensional visualization of neuronal networks in the whole mouse brain. *Nature Methods* **4**, 331 (2007).

14 Keller, P. J., Schmidt, A. D., Wittbrodt, J. & Stelzer, E. H. K. Reconstruction of Zebrafish Early Embryonic Development by Scanned Light Sheet Microscopy. *Science* **322**, 1065-1069 (2008).

15 Ahrens, M. B., Orger, M. B., Robson, D. N., Li, J. M. & Keller, P. J. Whole-brain functional imaging at cellular resolution using light-sheet microscopy. *Nature Methods* **10**, 413 (2013).

16 Ertürk, A. *et al.* Three-dimensional imaging of solvent-cleared organs using 3DISCO. *Nature Protocols* **7**, 1983 (2012).

17 Tomer, R., Ye, L., Hsueh, B. & Deisseroth, K. Advanced CLARITY for rapid and high-resolution imaging of intact tissues. *Nature Protocols* **9**, 1682 (2014).

18 Susaki, E. A. *et al.* Advanced CUBIC protocols for whole-brain and whole-body clearing and imaging. *Nature Protocols* **10**, 1709 (2015).

19 Pan, C. *et al.* Shrinkage-mediated imaging of entire organs and organisms using uDISCO. *Nature Methods* **13**, 859-867 (2016).

20 Fei, P. *et al.* Subvoxel light-sheet microscopy for high-resolution high-throughput volumetric imaging of large biomedical specimens. *Advanced Photonics* **1**, 016002 (2019).

21 Migliori, B. *et al.* Light sheet theta microscopy for rapid high-resolution imaging of large biological samples. *BMC biology* **16**, 57 (2018).

22 Voigt, F. F. *et al.* The mesoSPIM initiative: open-source light-sheet microscopes for imaging cleared tissue. *Nature Methods*, doi:10.1038/s41592-019-0554-0 (2019).

23 Fahrbach, F. O., Simon, P. & Rohrbach, A. Microscopy with self-reconstructing beams. *Nature Photonics* **4**, 780-785 (2010).

24 Planchon, T. A. *et al.* Rapid three-dimensional isotropic imaging of living cells using Bessel beam plane illumination. *Nature Methods* **8**, 417 (2011).

25 Gao, L., Shao, L., Chen, B. C. & Betzig, E. 3D live fluorescence imaging of cellular dynamics using Bessel beam plane illumination microscopy. *Nature Protocols* **9**, 1083-1101 (2014).

26 Chen, B. C. *et al.* Lattice Light Sheet Microscopy: Imaging Molecules to Embryos at High Spatiotemporal Resolution. *Science* **346**, 1257998 (2014).

27 Zhang, P., Phipps, M. E., Goodwin, P. M. & Werner, J. H. Light-sheet microscopy by confocal line scanning of dual-Bessel beams. *Journal of Biomedical Optics* **21**, 100502 (2016).

28 Zheng, G., Horstmeyer, R. & Yang, C. Wide-field, high-resolution Fourier ptychographic microscopy. *Nature photonics* **7**, 739 (2013).

29 Chhetri, R. K. *et al.* Whole-animal functional and developmental imaging with isotropic spatial resolution. *Nature Methods* **12**, 1171 (2015).

30 Medeiros, G. D. *et al.* Confocal multiview light-sheet microscopy. *Nature Communications* **6**, 8881 (2015).

31 Candes, E., Romberg, J. & Tao, T. Stable Signal Recovery from Incomplete and Inaccurate Measurements. *Communications on Pure & Applied Mathematics* **59**, 1207-1223 (2010).

32 Studer, V. *et al.* Compressive fluorescence microscopy for biological and hyperspectral imaging. *Proceedings of the National Academy of Sciences of the United States of America* **109**, 10136-10137 (2012).

33 Pavillon, N. & Smith, N. I. Compressed sensing laser scanning microscopy. *Optics Express* **24**, 30038 (2016).

34 Pascucci, M. *et al.* Compressive three-dimensional super-resolution microscopy with speckle-saturated fluorescence excitation. *Nature Communications* (2019).

35 Roy, S., Carass, A. & Prince, J. L. in *IEEE International Symposium on Biomedical Imaging: From Nano To Macro.* 101.

36 Preibisch, S., Saalfeld, S. & Tomancak, P. Globally optimal stitching of tiled 3D microscopic image acquisitions. *Bioinformatics* **25**, 1463-1465 (2009).

37 Preibisch, S., Saalfeld, S., Schindelin, J. & Tomancak, P. Software for bead-based registration of selective plane illumination microscopy data. *Nature methods* **7**, 418 (2010).

38 Yuste, R. The brain activity map: imaging the activity of entire neural circuits. *Bmc Neuroscience* **14**, 1-1 (2013).

39 Yin, X. *et al.* Spatial Distribution of Motor Endplates and its Adaptive Change in Skeletal Muscle. *Theranostics* (2019).

40 Pratt, S. J. P., Valencia, A. P., Le, G. K., Shah, S. B. & Lovering, R. M. Pre- and postsynaptic changes in the neuromuscular junction in dystrophic mice. *Frontiers in Physiology* **6**, 252 (2015).

41 Chang, B.-J. *et al.* Universal light-sheet generation with field synthesis. *Nature Methods* **16**, 235-238, doi:10.1038/s41592-019-0327-9 (2019).

42 Kim, S. J., Member, IEEE, Koh, K. & Lustig, M. An Interior-Point Method for Large-Scale `1-Regularized Least Squares. *IEEE Journal of Selected Topics in Signal Processing* **1**, 606-617 (2008).

43 Zhu, L., Zhang, W., Elnatan, D. & Huang, B. Faster STORM using compressed sensing. *Nature Methods* **9**, 721-723 (2012).

44 Qi, Y. *et al.* FDISCO: Advanced solvent-based clearing method for imaging whole organs. *Science advances* **5**, eaau8355 (2019).

45 Jing, D. *et al.* Tissue clearing of both hard and soft tissue organs with the PEGASOS method. *Cell research* **28**, 803 (2018).